Granular Flow in a Rotating Cone Partly Submerged in a Fluidized Bed

Arthur M. C. Janse, P. Maarten Biesheuvel, Wolter Prins, and Wim P. M. van Swaaij
Dept. of Chemical Technology, University of Twente, P.O. Box 217, 7500 AE Enschede, The Netherlands

When a rotating cone with supply openings near the bottom is partly inserted into a fluidized bed, solid particles are taken up and conveyed spirally over the inner surface. This principle for particle transport was used in a novel reactor for the flash pyrolysis of biomass with several distinct advantages. Particle velocities (up to 5 m/s) were measured, as well as the solids flow rate (up to 1.6 kg/s), as a function of the cone rotational velocity, cone size and cone top angle, the fluidization velocity, and the depth of the cone in the fluidized bed. Three hydrodynamic regimes were recognized, each with its own, specific flow characteristics influencing the particle residence time (distribution) on the cone wall and the solids flow rate. The transition between the regimes could be predicted using a force balance for a single particle. The particle velocity and residence time were modeled successfully for one of the regimes.

Introduction

The selective decomposition of organic material with a high molecular weight into products with a lower molecular weight often requires a high temperature (up to 900°C), a short residence time of reactants and products (in the order of seconds), and a high heat-transfer rate. This process is called flash pyrolysis and is applied for the following selective conversions:

- Coal to distillates (that is, oil) (Perry, 1997; p. 27−20; Kirk-Othmer, 1993, p. 582)
- Polymer to the corresponding monomer (Westerhout et al., 1998a,b)
- Biomass to bio-oil (Diebold and Bridgwater, 1997).

The bubbling and circulating fluidized bed are often used for these processes, because heat-transfer rates and temperatures are high, while the construction is relatively simple. However, particle- and gas-phase residence time may be too high (resulting in undesired cracking), while the large amount of carrier or fluidization gas necessitates an extra heat input and leads to larger downstream equipment. Another drawback may be the limiting mixing capacity of these reactors: the possible occurrence of cold zones near the feed entry points may cause nonoptimal process conditions.

Therefore, a novel reactor type was developed for the flash pyrolysis of biomass to (gaseous) bio-oil, based on a rotating cone (Wagenaar et al., 1994a,b, Figure 1. The organic material is added with an excess of hot inert particles to the heart of the rotating cone, and both particle types move spirally upward along the inner cone wall. When they fly over the edge, conversion of the organic material should be completed. The gaseous bio-oil is collected and cooled to obtain a liquid product.

This rotating cone reactor (RCR) can be operated at a high temperature with a low residence time of the biomass particles and the gaseous bio-oil. The heat transfer is high (Janse et al., 1999) and an auxiliary gas stream is in principle not needed, thereby preventing product dilution. Particles move in plug flow over the cone wall with product gases being removed in a cross-flow mode. Plug flow of the solids may prevent the development of cold zones, while rapid cross-flow removal of product vapors is advantageous to inhibit undesired secondary reactions (cracking) of the product vapors. This idea of cross-flow operation and rapid product removal is also applied in the work of Wolff et al. (1994), who experimented with a moving packed bed while applying a gas in cross-flow through the bed. Also, Krishna and Sie (1994) simulate plug flow of solids together with cross-flow of produced vapors in their reactor design for the pyrolysis of oil-shale, which consists of six fluidized-bed compartments in series in

Correspondence concerning this article should be addressed to A. M. C. Janse at his current address: DSM Food Specialties, P.O. Box 1, 2600 MA Delft, The Netherlands.

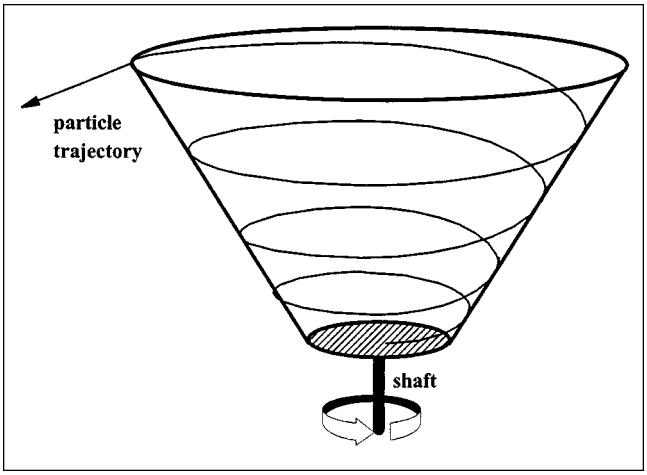

Figure 1. Original rotating cone principle without solids circulation.

Particles are added from above to the heart of the cone and spiral upward and out of the cone.

which the produced vapors are removed from each compartment.

To prevent secondary reactions of the products vapors, the gas-phase volume inside the cone can be reduced by the use of a stagnant inner cone. This element of the RCR is not considered here.

The first RCR could only be operated batchwise, but for continuous operation, the inert particles should be trapped and re-entered into the cone reactor. For this purpose, an alternative version of the rotating cone reactor was developed (Janse et al., 1997, 1998, 2000), which includes solids recycling (see Figure 2). In this design, the rotating cone is partly submerged into a fluidized bed and all particles enter the cone through one or more supply openings near the bottom of the cone. The rotation shaft can either be connected to the bottom of the cone, or mounted above the cone, thereby creating a single large supply opening at the bottom. In both designs, particles flow through the supply opening(s) upon cone rotation, and move upward along the cone wall in spiral pathways. After passing the upper edge, they fall back into the surrounding fluidized bed to close the solids circulation loop.

In this article, we describe the hydrodynamics of solids flow in the RCR with supply openings. The residence time of particles in the cone is considered, as well as the transport capacity (solids flow rate). These parameters are important, because the particle residence time limits the maximum size of the organic particles that are to be converted while the solids flow rate limits the amount of organic material that can be added to the cone without affecting the temperature of the heat-carrying (sand) particles.

Experiments in air and at room temperature are described with one type of sand only. In this work, the addition of organic particles and the resulting mixing is not considered. Cones of two sizes and two top angles are investigated with emphasis on the solids flow (from the fluidized bed into the cone) in the smaller cones and emphasis on the particle velocity and residence time (on the cone wall) in the larger cones. Theory is discussed which predicts the transitions between three flow regimes, based on a force balance over a single particle. From the same force balance, a model is derived which predicts the particle velocity in one of the regimes. To clarify the most important process parameters affecting the solids flow and the particle velocity, results of experiments are evaluated and compared with the theory.

Theoretical Background

The residence time of particles in the rotating cone can be predicted if all the forces acting on a single particle are known. These forces are gravity, particle-wall friction, the mutual friction between particles, the friction between particle and gas, and the so-called solids pressure which takes interparticle stress into account. The presence or absence of any of these forces is decisive for the hydrodynamic flow behavior. In this section, a criterion is developed to predict the conditions for which a certain flow type will develop. Subsequently, a model is presented from which the particle velocities for one of the flow regimes identified can be calculated. In the Results and Discussion section, the criterion and model are validated with experimental data.

Flow regimes on an inclined chute

The solids flow over the cone wall shows much resemblance with flow down a chute, which is simpler and, therefore, discussed first. The main difference is the presence of a centrifugal force in a rotating cone which results in particles moving upward instead of downward.

Although much research has been carried out on chute flow (an extensive review can be found in Savage, 1983), the flow behavior has not yet been classified into several well defined

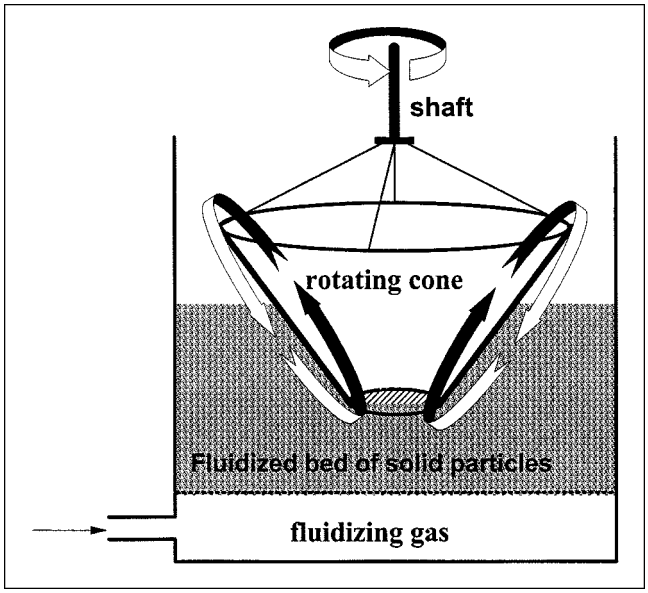

Figure 2. Rotating cone in which particles are circulated.

Here, the cone is driven from the top (cones 1 and 2), but the shaft can also be connected to the bottom of the cone (cones 3 and 4) (see Figure 4).

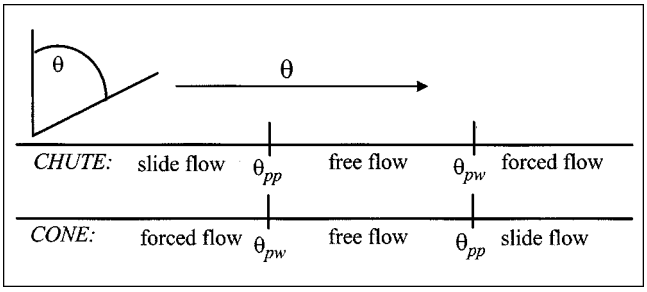

Figure 3. Flow regimes for chute flow and rotating cone flow.

regimes. Nevertheless, various models of increasing complexity are published. Savage (1979) proposed a viscosity model with four adjustable parameters to describe chute flow. With increasing computer power, models based on granular flow theory (Ocone et al., 1993) and discrete particle models (Zheng and Hill, 1996) also are applied. In this work, a much simpler approach is applied to define the hydrodynamic flow regimes on a chute and translate this to flow in a rotating cone.

A particle lying on a chute will flow downward by itself if the angle with the vertical θ is smaller than a critical value θ_{pw} (Figure 3). In that case, gravity is high enough to overcome the friction between the particles and the wall. This is called the free flow regime. Particles accelerate along the surface and the interparticle stress in r-direction (solids pressure) is zero. However, for $\theta > \theta_{pw}$, particle flow can only be induced by exerting an external force on the particles in r-direction which results in an interparticle stress. This is called ''forced flow''.

As long as θ is smaller than θ_{pw}, but larger than θ_{pp}, interparticle friction is not overcome and particles move in plug flow downward. However, for $\theta < \theta_{pw}$, particles slide over each other, resulting in a velocity gradient over the depth of the flowing layer ($dv_r/d\theta < 0$). The critical angle θ_{pp} represents the transition between the ''free flow'' and the ''slide flow'' regime. It is assumed here (as in the rest of the article) that the interparticle friction is higher than the friction of particles with the wall, that is, $f_{pp} > f_{pw}$. If this were not the case, the free flow regime would not exist, but instead the particle flow would be defined by zero wall slip ($v_{r,\text{wall}} = 0$) and a constant velocity gradient $dv_r/d\theta$ in the flowing layer.

The two critical angles θ_{pw} and θ_{pp} can be predicted from a force balance applied to a single particle. The normal force F_N, gravity F_g, and particle-wall friction F_w are incorporated in the balance, but particle-air friction is neglected (see further on). The result is:

$$\theta = \arctan\left(f^{-1}\right) \tag{1}$$

in which f represents the friction factor relating the friction force F_w to the normal force F_N

$$F_w = fF_N \tag{2}$$

To determine θ_{pw}, the particle-wall friction factor f_{pw} should be used, while the interparticle friction factor f_{pp} should be used for θ_{pp}. It was observed by Augenstein and Hogg (1974) that f_{pw} depends strongly on the surface roughness of the particle and the wall, but is independent of the velocity of the particle. In the same study, it was pointed out that f_{pw} is influenced by the particle diameter, whereas f_{pp} is not. Typical values of friction factors for particle flow along inclined surfaces are in the range of 0.4–0.7.

The above analysis is confirmed by several authors who determined the velocity profiles in sand layers moving along a chute. Savage (1979) observed plug flow with wall slip at a high θ (free flow regime), but measured a velocity gradient $dv_r/d\theta$ over the flowing layer combined with wall slip at lower θ ($v_{r,\text{wall}} \neq 0$, slide flow). Augenstein and Hogg (1978) also studied the flow of particles along chutes, and observed steep velocity gradient when the chute surface was coated with particles. However, when the chute surface was smooth and clean, a velocity gradient was only measured at a low θ.

Flow regimes in the rotating cone

For flow of particles along the rotating cone wall, the same two transition angles θ_{pw} and θ_{pp} can be obtained from a force balance over a single particle with the addition of the centrifugal force ($m_p\omega_p^2 x$). After rearrangement, an explicit expression for the critical particle rotational velocity (for a given angle θ) is found

$$\omega_p = \sqrt{\frac{g_y(\cos\theta + f\sin\theta)}{r\sin\theta(f\cos\theta - \sin\theta)}} \tag{3}$$

Here, g_y is the gravity acceleration ($= -9.81$ m/s^2) and r is the radial coordinate. From Eq. 3, values for the critical angles θ_{pw} and θ_{pp} (for a given velocity ω) are found by trial-and-error. Equation 3 equals Eq. 1 for $\omega = 0$, apart from a negative sign caused by the downward direction of the friction force for flow in the cone, while in chute flow, this force is oriented upward. At a sufficiently low cone angle θ (steep cone), a flow of solids can only be realized by means of a solids pressure from the fluidized bed in which the cone is submerged. This is the forced flow regime (see Figure 3). When the cone angle θ is increased, the centrifugal forces alone can become high enough to overcome the particle-wall friction and inertia forces. The particles accelerate over the cone wall and lose contact with each other (free flow regime). At an even higher cone angle θ, friction between particles is overcome as well and slide flow develops with a velocity gradient in the θ-direction (that is, over the depth of the flowing layer). A similar line of reasoning can be set up if the cone angle θ is not varied, but the particle rotational velocity ω_p.

Particle velocity in the free flow regime in the rotating cone

Of the three flow regimes, particle movement can be described most simply for the free flow regime, because particles move in plug flow without an interparticle stress in the r-direction (no solids pressure). For the forced flow regime, the solids pressure is present while the velocity gradient in θ-direction for the slide flow regime may also be difficult to describe. Therefore, only the free flow regime is modeled in this article. For this regime, particle movement along the cone

wall can be derived from a force balance over a single particle

$$m_p a_p = F_g + F_w + F_f + f_N \tag{4}$$

In Eq. 4, m_p stands for the mass of a particle and a_p stands for the acceleration of a particle. Interparticle stress in θ-direction S_θ (due to more inner layers pushing on more outward layers) is neglected in Eq. 4, although this is formally only correct for a monolayer of particles. However, S_θ can also be neglected for thicker layers, plug flow and absence of air friction. In the case of plug flow, a set of touching particles in the θ-direction can be considered a single rigid body with an undefined mass m_p and surface area A_p, but, if air friction can be neglected, the resulting Eqs. 11, 12 and 13 show that m_p and A_p do not influence the particle velocity.

Besides, we will argue in the Results and Discussion section that qualitative arguments and experimental results indicate that air friction can be neglected for thick layers and only has to be included for very dilute (mono-)layers. For these thin layers, S_θ is (close to) zero.

This first term on the righthand side of Eq. 4 represents gravity

$$F_g = m_p g \tag{5}$$

The friction force between particle and wall depends linearly on the normal force (see Eq. 2)

$$F_w = -\, f_{pw} F_N \frac{(\boldsymbol{v}_w - \boldsymbol{v}_p)}{|\boldsymbol{v}_w - \boldsymbol{v}_p|} \tag{6}$$

Here, $\boldsymbol{v}_w$ is the velocity of the cone wall and $\boldsymbol{v}_p$ the particle velocity.

The third term takes into account the viscous friction between the particle and the surrounding air

$$F_f = C_D A_p \frac{1}{2} \rho_g |\boldsymbol{v}_g - \boldsymbol{v}_p| (\boldsymbol{v}_g - \boldsymbol{v}_p) \tag{7}$$

Here, A_p is the particle cross-sectional surface and ρ_g the gas density (1.205 kg/m^3).

An expression by Rowe (1961) is used for the drag coefficient C_D

$$C_D = \frac{24}{\mathrm{Re}_p}\left(1 + 0.15\mathrm{Re}_p^{0.687}\right) \qquad \mathrm{Re}_p = \frac{d_p \rho_g |\boldsymbol{v}_p - \boldsymbol{v}_g|}{\eta_g} < 1{,}000 \tag{8}$$

Here, η_g is the gas viscosity ($18.1 \cdot 10^{-6}$ Pa·s).

The fourth term of Eq. 4 represents the normal force exerted by the cone wall onto the particle in the direction perpendicular to the cone wall

$$F_N = F_N e_\theta \tag{9}$$

Equations 4–9 were written out for a spherical coordinate system (r, θ, φ) with g_y parallel to the $\theta = 0$-axis and $v_\theta = 0$, which results in the following expressions for the particle velocities in r- and φ-direction (v_r and v_φ)

$$\frac{dv_r}{dr} = \frac{1}{v_r}\left\{ -\frac{f_{pw} F_N v_r}{m_p \sqrt{v_r^2 + \left[r \sin\theta(\omega_w - \omega_p)\right]^2}} + g_y \cos\theta + r \sin^2\theta \omega_p^2 - \frac{C_D A_p \rho_g v_r \sqrt{v_r^2 + \left[r \sin\theta(\omega_w - \omega_p)\right]^2}}{2 m_p} \right\} \tag{11}$$

$$\frac{d\omega_p}{dr} = \frac{1}{v_r}\left\{ \frac{f_{pw} F_N (\omega_w - \omega_p)}{m_p \sqrt{v_r^2 + \left[r \sin\theta(\omega_w - \omega_p)\right]^2}} - \frac{2 v_r \omega_p}{r} + \frac{C_D A_p \rho_g (\omega_w - \omega_p) \sqrt{v_r^2 + \left[r \sin\theta(\omega_w - \omega_p)\right]^2}}{2 m_p} \right\} \tag{12}$$

$$F_N = m_p \left\{ r \sin\theta \cos\theta \omega_p^2 - g_y \sin\theta \right\} \tag{13}$$

$$\mathrm{Re}_p = \frac{d_p \rho_g \sqrt{v_r^2 - \left[r \sin\theta(\omega_w - \omega_p)\right]^2}}{\eta_g} \tag{14}$$

Here, ω_p and ω_w are the rotational velocities of particle and wall (rad/s), related to the tangential velocities (m/s) by $v_\varphi = \omega \cdot \sin\theta \cdot r$. In the above equations, it is assumed that the gas velocity in r-direction is zero and equals the wall velocity in φ-direction. Differential Eqs. 11 and 12 were solved by a fourth-order Runge Kutta technique with step size adjustment. The radial velocity of the particles at the entrance to the cone r_{in} is set to zero ($v_{r,\mathrm{in}} = 0$). For the rotational velocity ω_p at r_{in}, the minimal value at which a particle is able to move upward ($v_r > 0$) is used, which follows from Eq. 3 with $r = r_{\mathrm{in}}$ and $f = f_{pw}$. The residence time τ on the cone wall follows from

$$\tau = \int_{r_{\mathrm{in}}}^{r_{\mathrm{out}}} v_r^{-1} dr \tag{15}$$

Experimental Studies

Setup

Experiments at room temperature and atmospheric pressure were carried out with four different cones (for dimensions see Table 1) submerged at various depths in beds fluidized by air. The cone rotational velocity and fluidizing gas velocity were varied. Two of the cones are small (typical dimension 10 cm, No. 1 and 2) and have a single sand supply opening (see Figure 2). The other two (see Figure 4, No. 3 and 4) are larger (30–60 cm), and have four supply openings and a shaft at the bottom of the cone. This design makes the cones easily accessible from the top, which may be advantageous for experiments. However, the rotating shaft is now within the fluidized bed, which necessitates the use of a so-called labyrinth sealing which is flushed with air. Of each set

Table 1. Overview of Rotating Cones

Cone No.	1	2	3	4
Half cone top angle θ (°)	43.5	32.0	45	30
Cone bottom diameter (cm)	2.9	3.2	22	14
Cone top diameter (cm)	10.4	10.9	68	28
Number of transport openings	1	1	4	4
Area per opening (cm^2)	6.6	8.0	65	33
Transition forced flow to free flow (Hz)	4.1–7.8	8.0–14.8	1.5–2.7	7.0–9.9
Transition free flow to slide flow (Hz)	5.7–10.7	∞	2.1–3.6	∞

of cones, one cone has a half cone top angle θ of 45° and for the other $\theta = 30°$.

Measurements

Cones were submerged in a fluidized bed and flow rate and particle velocities were measured for the large cones (3 and 4). In the small cones (1 and 2), the flow rate was adjusted by controlling the outflow from a sand silo mounted on top of the equipment, and the sand level difference between the fluidized bed surrounding the cone and inside the cone was measured. In these experiments, the sand flowing over the top rim of the cone is collected in a separate outer basket.

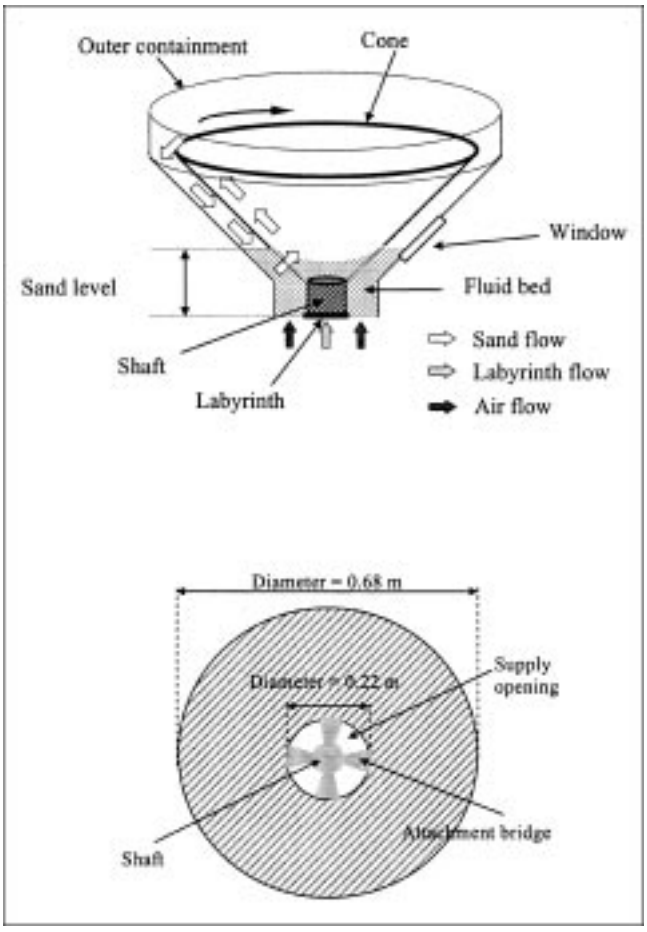

Figure 4. Cone with the shaft connected to the bottom with four supply openings (No. 3, Table 1).

For cones 3 and 4, the velocity of particles flowing over the cone wall was measured using a video camera. Fluorescent marker particles were followed in the cone, while UV-light was used to enhance the contrast with the surrounding sand particles. There are three options to determine the radial and rotational velocity (v_r, v_φ) of the marker particles directly with a video camera system:

(1) Measuring the particle coordinates in two subsequent video snapshots. The particle velocity can be determined from the displacement and the time between the snapshots.

(2) Counting the number of snapshots required for a particle to make a full rotation in the cone, which gives v_φ directly. By measuring the translation in r-direction, v_r follows. This technique is possible when only a few marker particles are added.

(3) At high particle velocities, the movement of a particle on a snapshot is pictured as a streak. A combination of line length (in two directions) and snapshot duration time gives the particle velocity.

For cone 3, method 1 was used for v_r and method 3 for v_φ. For cone 4, method 2 was used for v_φ, but none of the above methods could be used for v_r. This was caused by the low value of the radial velocity, which resulted in a large measurement error. Therefore, an indirect technique was used for v_r based on the measurement of the mass-flow rate ϕ_s and the cross-sectional area available for solids flow. Now, v_r follows from

$$v_r = \frac{\phi_s}{2\pi r \sin\theta \delta_\theta \rho_s (1-\epsilon)} \tag{16}$$

Here, ϕ_s is the solids flow rate (kg/s), δ_θ is the layer thickness in θ-direction, ρ_s is the density of the solids, and ϵ is the porosity of the flowing layer. The layer thickness δ_θ was determined using a plumbline that was let down into the rotating cone from a certain reference height until it hit the flowing sand layer. Before the experiments, the ''depth'' of the cone wall was determined. Subtracting these values gives the layer thickness δ_y in a vertical direction. The layer thickness δ_θ is given by $\delta_\theta = \delta_y \cdot \sin\theta$.

The solids flow rate ϕ_s over the cone wall is determined for the larger cones by collecting a well-defined part of the sand flow over the top during a certain fixed period of time (see Figure 5). This is realized by placing a small basket in the direction of flow inside the perimeter of the outer containment. The flow rate measured is divided by the fraction of the total perimeter occupied by the basket to give the total flow rate ϕ_s.

The particle residence time τ on the cone wall can be determined from a set of n measurements $(r_i, v_{r,i})$ by writing the integral (Eq. 15) as a summation: $\tau = \sum_{i=1}^{n} (\Delta r_i / v_{r,i})$. Points at the lower end of the cone r_{in} and the top r_{out} must be part of this set.

Sand properties

The properties of the sand particles are given in Table 2. The friction factors were determined by experiments on a

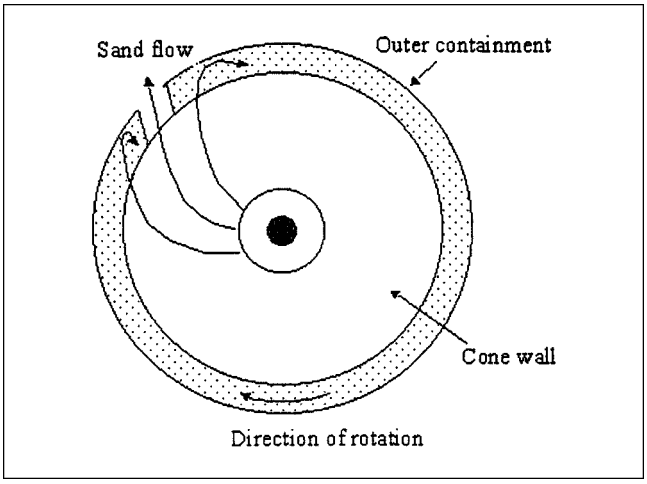

Figure 5. Measurement of sand transport capacity.

chute (see Eq. 1). The measured friction factors are in good agreement with those reported by Augenstein and Hogg (1974), who found values of 0.53 and 0.74 for particle-wall and interparticle friction (similar particle size).

Results and Discussion

In this section, first observations are described that elucidate the picture of a forced flow and a free flow regime. Secondly, measurements of the bed level difference inside and outside of the cone are presented for the small cones. Thirdly, measured and calculated particle velocities for the free flow regime are compared for cone 3. Fourth, measurements on flow rate and particle velocity are presented for the forced flow regime (cone 4), and it is argued that a prediction of the observed velocities and flow rate is still not possible for this regime.

Identification of flow regimes

In the Theoretical Background, it was postulated that three hydrodynamic flow regimes exist for flow over the cone wall. In the free flow regime, the centrifugal force is sufficiently high to transport particles in an upward direction along the cone wall by itself. A solids pressure is absent and as a consequence, the residence time of particles on the cone wall is only a function of the cone rotational frequency and characteristic cone dimensions (see Table 3). The transport capacity of solids is completely determined by the transport resistance in the supply openings.

In contrast, the resistance for transport of solids in the forced flow regime is situated in the supply openings combined with the resistance along the cone wall. Solids flow, particle velocity, and residence time are all determined by both the resistance in the transport openings, and the characteristics of the cone.

Experimental work in cone 3 confirms these ideas (see Figure 6). Up to rotational frequencies of 2.2–2.4 Hz (cone rotational frequency = $\omega_w/(2\pi)$), the transport rate increases with higher cone velocities (forced flow regime), whereafter the transport rate flattens out to a nearly constant value of approximately 1.5 kg/s (free flow). The critical value for the change in flow regime can be calculated from Eq. 3 as 1.5–2.7 Hz which is in agreement with the measured transition (see Table 1).

It must be emphasized that the transition between flow regimes depends on the location on the cone wall and is not a unique value (see Eq. 3). On increasing the cone velocity, the transition from forced to free flow occurs at the top of the cone wall r_{out} first, while for $r < r_{out}$, transport is in the forced flow regime. With increasing cone velocity, the transition moves downward until the sand inlet point r_{in} is reached and the entire sand layer is in the free flow regime.

According to Eq. 3, in experiments in the forced flow regime the transport of solids stops when the external force (the solids pressure) is taken away by interrupting the gas flow to the fluidized bed or by lowering the solids holdup in the bed (reducing the bed height). In that case, a stagnant sand layer resides on the rotating cone wall. In experiments in the free flow regime (according to Eq. 3), the cone is emptied completely when the supply of solids was stopped. Stag-

Table 2. Physical Properties of the Sand Particles

Average particle diameter d_p	390 μm (200—500 μm)
Density ρ_s	2,605 kg/m^3
Minimum fluidization velocity U_{mf}	0.08 m/s
Packed bed porosity ϵ	0.4
Particle-wall friction factor f_{pw}	0.53
Interparticle friction factor f_{pp}	0.71

Table 3. Differences between the Free Flow and the Forced Flow Regime

	Free Flow	Forced Flow
Acceleration of particles in *r*-direction?	Yes	No
Velocity in *r*-direction?	High	Low
Slip in φ-direction between particle and cone wall?	Yes	No
Resistance to solids flow in	Transport openings only	Transport openings and
Particle velocity on cone determined by	Cone characteristics only	on cone wall

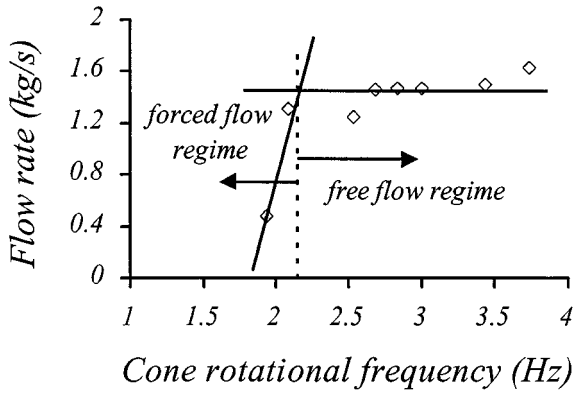

Figure 6. Transition in flow regime (cone 3) from measurements on solids flow rate ϕ_S.

Superficial gas velocity 0.37 m/s.

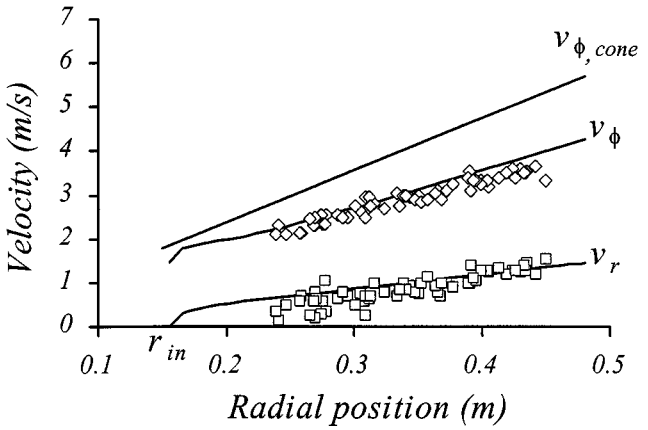

Figure 7. Measured (symbols) and calculated (lines) particle velocity in radial and tangential direction (v_r and v_φ) as a function of the radial position for the free flow regime (cone 3).

Cone rotational frequency = 2.68 Hz; superficial gas velocity 0.37 m/s.

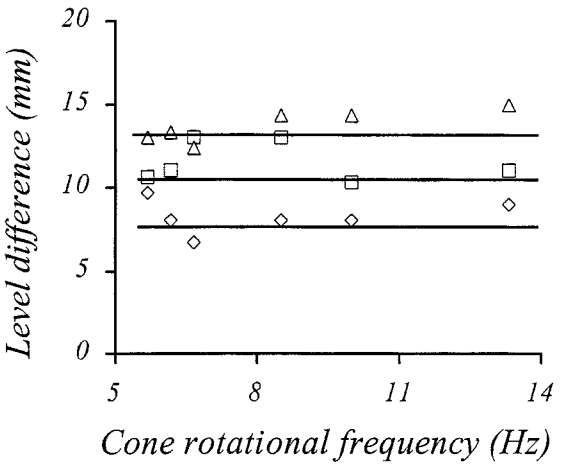

Figure 9. Measured sand level difference between the fluidized bed surrounding the rotating cone and the fluidized bed inside the cone as a function of the cone rotational frequency and solids flow rate ϕ_s. ◇ 27 kg/h; □ 48 kg/h; △ 62 kg/h (cone 1, superficial air velocity 0.07 m/s). Lines are trendlines.

nant sand layers never developed. These results support the theory of different flow regimes.

Typical examples of the free and forced flow regime are depicted in Figures 7 and 8, respectively. These two figures clearly show several different characteristics based on the presence or absence of the solids pressure (see Table 3).

Free and forced flow in the small cones

For a constant flow rate, the bed level difference between the inside and the outside of the cone automatically adjusts itself to a stationary value, which is a measure of the driving force necessary to overcome the friction forces when particles flow into the center of the cone. Figures 9 and 10 show the influence of the cone rotational frequency and the solids flow rate on the bed level difference between the inside and the outside of the cone. As illustrated in Figure 9 for cone 1, the sand level difference is roughly independent of the cone velocity which suggests that the resistance to solids flow is entirely located in the supply openings (free flow regime). However, for frequencies up to 9 Hz in the steeper cone 2 (Figure 10), the sand level difference decreases when the cone rotational frequency is increased, which indicates that the cone wall velocity is also rate-limiting (forced flow regime). At frequencies above 9 Hz, the level difference is again inde-

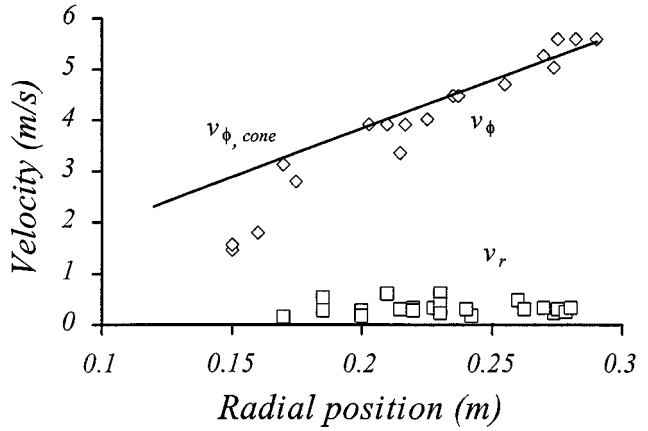

Figure 8. Measured particle velocity in radial and tangential direction (v_r and v_φ) as a function of the radial position for the forced flow regime (cone 4).

Cone rotational frequency = 6.12 Hz and the pressure in the fluidized bed at the height of the solids supply openings is 900 Pa. Superficial gas velocity 0.12 m/s.

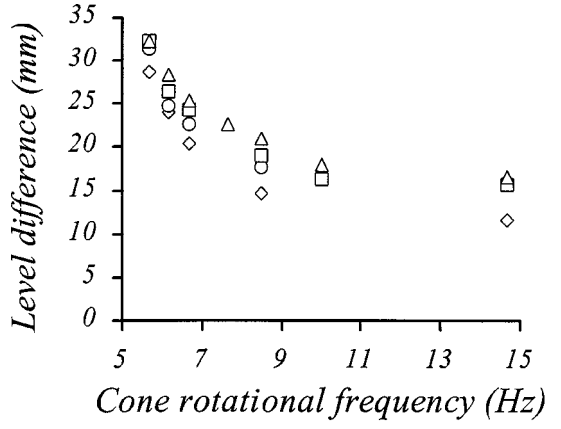

Figure 10. Measured sand level difference between the fluidized bed surrounding the rotating cone and the fluidized bed inside the cone as a function of the cone rotational frequency and solids flow rate ϕ_s.

◇ 27 kg/h; ○ 34 kg/h □ 48 kg/h, △ 62 kg/h (cone 2, superficial air velocity 0.07 m/s).

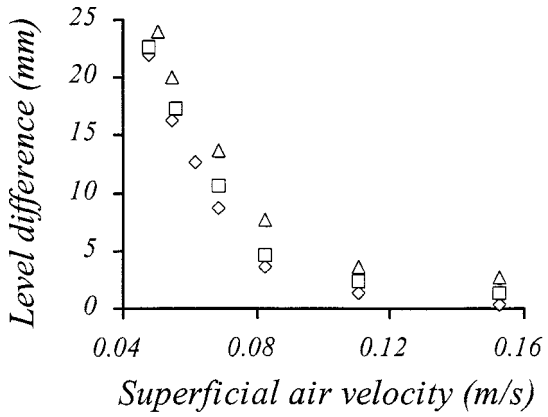

Figure 11. Measured sand level difference between the fluidized bed surrounding the rotating cone and the fluidized bed inside the cone as a function of the superficial air velocity and solids flow rate ϕ_s (Figure 10) (cone 1, frequency = 8.5 Hz).

Resistance to flow vanishes above the minimum fluidization velocity (U_{mf} = 0.08 m/s).

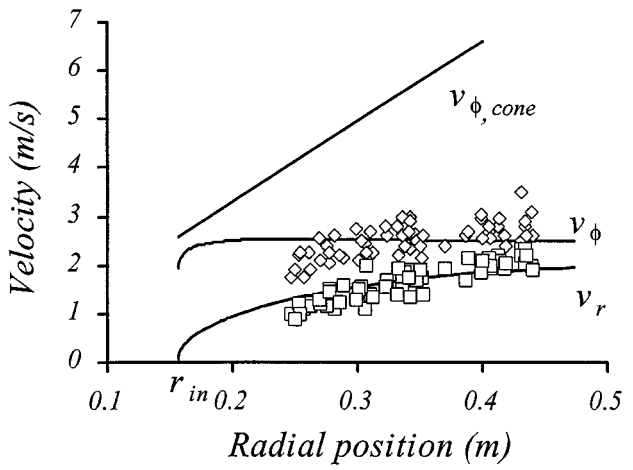

Figure 12. Comparison between the experimentally determined particle velocities (symbols) in r- and φ-direction and model predictions (lines) at a cone rotational frequency of 3.73 Hz for cone 3.

Superficial gas velocity 0.37 m/s.

pendent of frequency (free flow). The measured transition is within the calculated range 8.0–14.8 Hz (see Table 1).

Figure 11 shows the sand level difference as a function of the gas velocity to the fluidized bed. Clearly, the required driving force (the sand level difference) for sand flow from bed to cone vanishes when approaching the minimum fluidization velocity U_{mf} and flattens out beyond that point because interparticle resistance strongly decreases above U_{mf}.

Free and forced flow in the large cones

Particle velocities in the free flow regime can be calculated using the single particle model discussed in the Theoretical Background. Experimental results and model predictions are compared in Figure 7 and 12 for cone rotational frequencies of 2.68 and 3.73 Hz. For 2.38 Hz, a similar figure was obtained as for 2.68 Hz. At the highest frequency (Figure 12), measurements were described accurately when the measured friction factor f_{pw} was used (see Table 2) and the particle-air friction F_f was omitted from the model. In contrast, for the two lowest frequencies, best results were obtained when F_f was included in the model and if a much lower particle-wall friction factor f_{pw} was used ($f_{pw} = 0.33$) for F_w than actually measured on a chute (Figure 7). This result is in agreement with visual observations of the flowing layers: for the highest frequency, the flowing layer was thick in contrast to the very dilute layers that formed at the lowest frequencies. For the thick layer, a large fraction of the particles is not at the particle-air interface and, therefore, not influenced by friction with the air, which validates omitting the particle-air friction F_f. Furthermore, for a dilute layer, particles do not touch. This allows a rolling motion instead of the measured sliding motion (Table 2) for which obviously the friction factor is much lower.

Figures 7 and 12 further show that with increasing cone velocity the radial velocity v_r increases (for a given radial position), while the difference between the velocity of the cone wall and the particle velocity v_φ increases. An explanation is the fact that at higher cone velocity it becomes gradually more difficult for particles to follow the movement of the cone wall due to the inertia forces. As a consequence, particle-wall slip will increase. Simultaneously, higher cone velocities induce higher centrifugal forces which increase the upward oriented centrifugal force component, which results in higher radial velocities v_r.

For the two sets of inputs ($f_{pw} = 0.53$ and no air friction; $f_{pw} = 0.33$ with air friction), the calculated residence time is depicted in Figure 13. Above a critical frequency, the residence time quickly decreases to a more or less constant value.

Figure 14 shows the calculated residence time as a function of the (half cone) top angle θ. A minimum in residence time is found at $\sim \pi/4$ rad. Obviously, at this angle the nega-

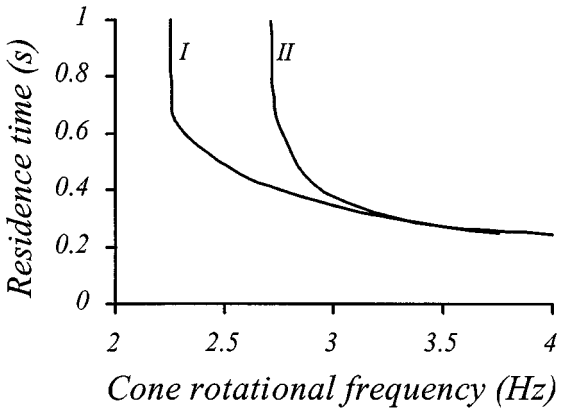

Figure 13. Modeled particle residence time for cone 3.

Case I: $f_{pw} = 0.33$, air friction; Case II: $f_{pw} = 0.53$, no air friction.

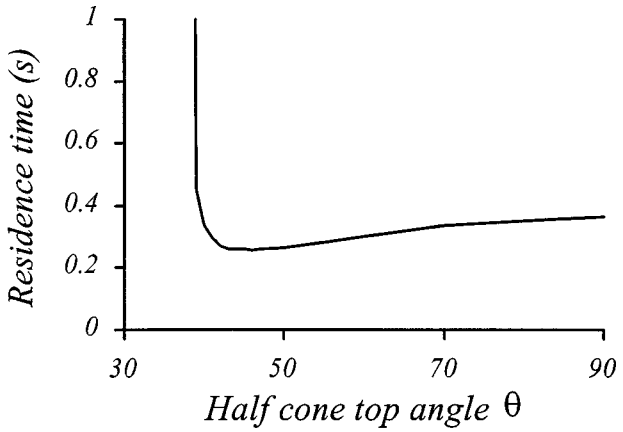

Figure 14. Modeled residence time as function of cone angle θ for cone 3 and a frequency of 3.73 Hz, a friction factor of 0.53 and no air friction.

tive influence of the wall friction F_w on v_r (see Eq. 11) is balanced by the positive effect of F_w on v_φ (and, therefore, indirectly on v_r). It is interesting to note that the model predicts a lower residence time for a rotating cone of typically $\pi/4$ rad than for the rotating disk reactor ($\theta = \pi/2$).

Figure 8 shows the measured particle velocities in the r- and φ-direction for the forced flow regime for a frequency of 6.12 Hz (cone 4). Similar results were obtained for a frequency of 5.34 and 6.9 Hz. For the same cone and the same range of frequencies, the measured residence time of particles is depicted in Figure 15 as a function of the cone rotational frequency and the fluidized-bed pressure at the height of the supply openings. The residence time depends on the bed pressure which indicates again that measurements were in the forced flow regime. The figure shows that, especially at high rotational frequencies (> 6 Hz), variation of the bed

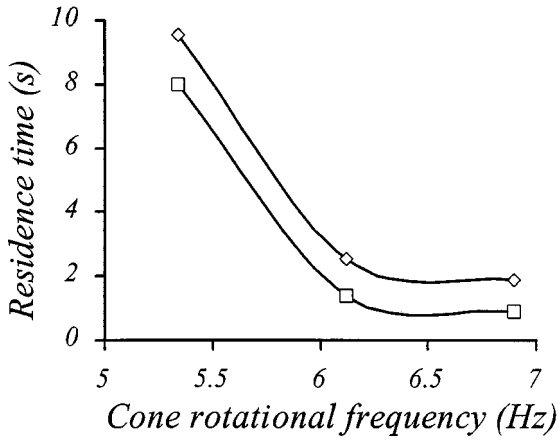

Figure 15. Measured residence time of particles in cone 4 as function of the cone rotational frequency in the forced flow regime for two different bed pressures at the height of the solid supply openings ◇ 900 Pa, □ 1,000 Pa.

Superficial gas velocity 0.12 m/s. Lines are trendlines.

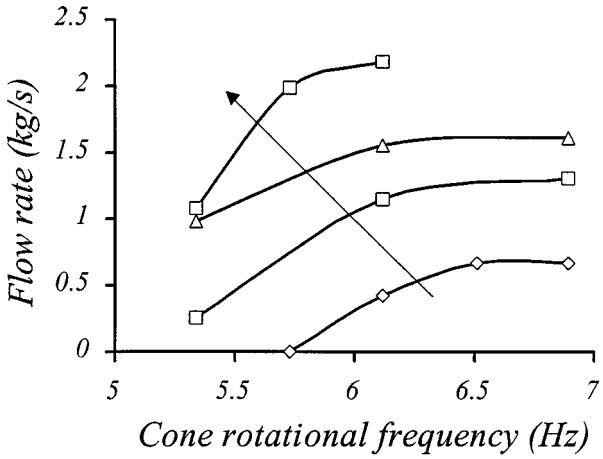

Figure 16. Measured mass-flow rate as function of the cone rotational frequency (cone 4) and pressure in fluidized bed at the height of the solid supply openings.

Pressure increases in the direction of the arrow (790, 840, 1,015 and 1,200 Pa). Superficial gas velocity 0.12 m/s. Lines are trendlines.

pressure with only 10% can alter the residence time with more than 50%. The solids flow rate as a function of the cone rotational frequency and bed pressure is depicted in Figure 16 for cone 4. The flow rate depends on the frequency, which again shows that measurements were in the forced flow regime, in accordance with the predicted transition to free flow in the 7.0–9.9 Hz range (see Table 1).

Particle velocities on the cone wall could not be calculated in the forced flow regime. According to calculations without the solids pressure, no solids transport could take place, because ω_p is below the critical velocity. Therefore, to calculate particle velocities on the cone wall in the forced flow regime, the solids pressure should be included in the model. The solids pressure depends on the fluidized-bed pressure at the height of the supply opening(s), but the exact nature of this dependence is unknown. Similar difficulties arise if it is desired to model the solids flow rate. For the free flow regime, this may succeed if the supply opening is looked at as an orifice between two fluidized beds (Korbee et al., 1994). For the forced flow regime, this is, again, more difficult because of the unknown value of the solids pressure at the inside of the supply opening(s).

Conclusions

A novel rotating cone reactor was tested for the flash pyrolysis of biomass. In this design, the rotating cone is placed in a fluidized bed, while solids flow through one or more supply openings in the cone wall. Particle velocities and solids flow rate could be measured adequately in experiments at room temperature and atmospheric pressure. A large flow of granular material was realized (up to 1.6 kg/s) in cones with typical dimensions of 0.5 m or less, while particle residence times were as low as 0.1 s. Three hydrodynamic regimes were identified for flow of (thick) layers of granular material along an inclined surface, and a criterion for the transition between

the regimes is derived. Literature data on chute flow could differentiate between the free flow regime and the slide flow regime, while experiments with rotating cones revealed a difference between the free flow and the forced flow regime.

In the free flow regime, a good prediction of particle velocities is possible. In the case of forced flow, this is still not possible because of the unknown value of the solids pressure.

Acknowledgments

This investigation was supported by the European Community (CEC-AIR CT93-0889). We thank H. Weerdenburg, J. Nijmeijer, G. Schorfaar and O. D. Veehof for their assistance in the theoretical and experimental work.

Literature Cited

Augenstein, D. A., and R. Hogg, ''Friction Factors for Powder Flow,'' *Powder Tech.*, **10**, 43 (1974).

Augenstein, D. A., and R. Hogg, ''An Experimental Study of the Flow of Dry Powders over Inclined Surfaces,'' *Powder Tech.*, **19**, 205 (1978).

Diebold, J. P., and A. V. Bridgwater, ''Overview of Fast Pyrolysis of Biomass for the Production of Liquid Fuels,'' *Developments in Thermochemical Biomass Conversion*, A. V. Bridgwater, and D. G. B. Boocock, eds., Blackie Academic, London, p. 5 (1997).

Janse, A. M. C., W. Prins, and W. P. M. Van Swaaij, ''Development of a Small Integrated Pilot Plant for Flash Pyrolysis of Biomass,'' *Developments in Thermo-chemical Biomass Conversion*, A. V. Bridgewater and D. G. B. Boocock, eds., Blackie Academic, London, p. 368 (1997).

Janse, A. M. C., ''A Heat Integrated Rotating Cone Reactor System for Flash Pyrolysis of Biomass,'' Thesis, University of Twente, The Netherlands (1998).

Janse, A. M. C., X. A. De Jong, W. Prins, and W. P. M. Van Swaaij, ''Heat Transfer Coefficients in the Rotating Cone Reactor,'' *Powder Tech.*, **106**, 168 (1999).

Janse, A. M. C., P. M. Biesheuvel, W. Prins, and W. P. M. Van Swaaij, ''A Novel Interconnected Fluidized Bed for the Combined Flash Pyrolysis of Biomass and Combustion of Char,'' *Chem. Eng. J.*, **76**, 77 (2000).

Kirk-Othmer, *Encyclopedia of Chemical Technology*, 4th ed., Vol. 6, Wiley, New York (1993).

Korbee, R., O. C. Snip, J. C. Schouten, and C. M. Van der Bleek, ''Rate of Solids and Gas Transfer via an Orifice between Partially and Completely Fluidized Beds,'' *Chem. Eng. Sci.*, **49**, 5819 (1994).

Krishna, R., and S. T. Sie, ''Strategies for Multiphase Reactor Selection,'' *Chem. Eng. Sci.*, **49**, 4029 (1994).

Ocone, R., S. Sundaresan, and R. Jackson, ''Gas-Particle Flow in a Duct of Arbitrary Inclination with Particle-Particle Interactions,'' *AIChE J.*, **39**, 1261 (1993).

Perry, R. H., *Perry's Chemical Engineers' Handbook*, 7th ed., McGraw-Hill, New York (1997).

Pilpel, N., ''Flow Properties of Non-Cohesive Powder,'' *Chem. Process. Eng.*, **46**, 167 (1965).

Rowe, P. N., ''Drag Forces in a Hydraulic Model of a Fluidised Bed, Part 1.,'' *Trans. Inst. Chem. Engrs*, **39**, 43 (1961).

Savage, S. B., ''Gravity Flow of Cohesionless Granular Materials in Chutes and Channels,'' *J. Fluid Mech.*, **92**, 53 (1979).

Savage, S. B., ''The Flow of Granular Materials III: Rapid Shear Flows,'' *Chem. Eng. Sci.*, **38**, 189 (1983).

Wagenaar, B. M., J. A. M. Kuipers, and W. P. M. Van Swaaij, ''Particle Dynamics and Gas Phase Hydrodynamics in a Rotating Cone Reactor,'' *Chem. Eng. Sci.*, **49**, 927 (1994a).

Wagenaar, B. M., W. Prins, and W. P. M. Van Swaaij, ''Pyrolysis of Biomass in the Rotating Cone Reactor: Modelling and Experimental Justification,'' *Chem. Eng. Sci.*, **49**, 5109 (1994b).

Westerhout, R. W. J., J. Waanders, J. A. M. Kuipers, and W. P. M. Van Swaaij, ''Recycling of Polyethene and Polypropene in a Novel Bench-Scale Rotating Cone Reactor by High-Temperature Pyrolysis,'' *Ind. Eng. Chem. Res.*, **37**, 2293 (1998a).

Westerhout, R. W. J., J. Waanders, J. A. M. Kuipers, and W. P. M. Van Swaaij, ''Development of a Continuous Rotating Cone Reactor Pilot Plant for the Pyrolysis of Polyethene and Polypropene,'' *Ind. Eng. Chem. Res.*, **37**, 2316 (1998b).

Wolff, E. H. P., P. Veenstra, and L. A. Chewter, ''A Novel Circulating Cross-Flow Moving Bed Reactor System for Gas-Solids Contacting,'' *Chem. Eng. Sci.*, **49**, 5427 (1994).

Zheng, X. M., and J. L. Hill, ''Molecular Dynamics Modelling of Granular Chute Flow: Density and Velocity Profiles,'' *Powder Tech.*, **86**, 219 (1996).

Manuscript received Apr. 26, 1999 and revision received Aug. 3, 1999.